

## Synthesis of Powdered $[\text{Mn}(\text{bipy})_3](\text{CF}_3\text{SO}_3)_2 \cdot 5.5\text{H}_2\text{O}$ : The Physical Properties and Antibacterial Activity

Kristian Handoyo Sugiyarto\*, Dwi Anggi Marini, Hari Sutrisno, Dyah Purwaningsih, and Cahyorini Kusumawardani

Department of Chemistry Education, Universitas Negeri Yogyakarta, Jl. Colombo No. 1, Yogyakarta 55281, Indonesia

\* **Corresponding author:**

tel: +62-8157935534

email: sugiyarto@uny.ac.id

Received: September 6, 2022

Accepted: December 15, 2022

DOI: 10.22146/ijc.77565

**Abstract:** The synthesis of the complex containing manganese(II), bipyridine (bipy) as a ligand, and an anionic trifluoromethane sulfonate (triflate) is reported. The corresponding metal content, conductance, and DTG-TGA of the complex lead to the formula of  $[\text{Mn}(\text{bipy})_3](\text{triflate})_2 \cdot 5.5\text{H}_2\text{O}$ . The fully high-spin magnetic moment is observed, corresponding to five unpaired electrons in the metal ion. The electronic spectral bands suggest the three possible spin-forbidden transitions of the sextet to quartet states. The mode of vibrations of the IR spectrum supports the typical ring of bipy, and the triflate. The images of SEM-EDX indicate the presence of the corresponding elemental content and reflect the relatively high crystallinity, as it is evidenced in the profile of the corresponding powdered diffractogram. The refinement of powdered XRD following the Le Bail program suggests being structurally triclinic symmetry of  $P_{21}/c$ . This complex shows inhibition of bacterial activity against *S. aureus* and *E. coli*.

**Keywords:** manganese(II); bipyridine; triflate; PXRD; antibacterial

### ■ INTRODUCTION

The chemistry of six coordinated bidentate, phenanthroline (*phen*), and bipyridine (*bipy*), of divalent metals such as Mn(II), Co(II), Ni(II), and Cu(II) with various counterpart anions have been much well studied concerning P-XRD [1-7]. Among the divalent metal complexes, not many detailed physical properties are previously reported, and Mn(II) might exhibit an important role in the development of metal-based drugs. The development of chemotherapeutic organic bases and their metal complexes is now attracting the attention of medicinal chemists [8]. A possible idea for the toxicity of the complexes has been proposed in terms of the chelation theory [9]. Thus, preparation of solid Mn(II) containing *tris-bipy* with triflate anion is a challenge, and the results in its magnetism, IR-UV-Vis spectral properties, Powder-XRD, and anti-bacterial-activity against *Staphylococcus aureus* (*S. aureus*) and *Escherichia coli* (*E. coli*) are reported. The characteristics of the two bacteria represent the two types of gram-positive and gram-negative, respectively. They have been long recognized to be a pathogen, very

famous, and easily found in the surrounding of human life causing disease, skin, and soft tissue infections. In particular, the *E. coli* infection leads to (bloody) diarrhea, vomiting, stomach pains, and cramps. Therefore, the anti-bacterial activity of the complex will be readily known being able to kill both or only one of them, or only inhibit the growth of both or only one of them.

### ■ EXPERIMENTAL SECTION

#### Materials

The main reagents, manganese(II) nitrate tetrahydrate- $\text{Mn}(\text{NO}_3)_2 \cdot 4\text{H}_2\text{O}$  (97%), 2,2'-bipyridine (99%), and potassium trifluoromethanesulfonate- $\text{KCF}_3\text{SO}_3$  (98%), for the complex preparation, and sodium sulfate- $\text{Na}_2\text{SO}_4$  (99.99%), ammonium chloride- $\text{NH}_4\text{Cl}$  (99.5%), manganese(II) sulfate monohydrate- $\text{MnSO}_4 \cdot \text{H}_2\text{O}$  (99.99%), aluminum nitrate nonahydrate- $\text{Al}(\text{NO}_3)_3 \cdot 9\text{H}_2\text{O}$  (98%), iron(III) chloride- $\text{FeCl}_3$  (reagent grade, 97%), and potassium chloride-KCl (99.09%), for conductivity measurement, were obtained from Aldrich-Sigma, and directly used without special treatment. The Nutrient

Agar (NA), Nutrient Broth (NB), Chloramphenicol, bacteria *E. coli* and *S. aureus*, for antibacterial testing, were obtained from the Microbiological Laboratory, Department of Biology, Yogyakarta State University.

### Instrumentation

The instrumentations used in this study were UV-Vis spectrophotometer (Pharmaspec UV 1700), Magnetic Susceptibility Balance (Auto Sherwood Scientific 240V-AC), Fourier-Transformed Infrared Spectrophotometer (FTIR-ABB MB3000 Specord 100), Atomic Absorption Spectrophotometer (PinAAcle 900T Perkin Elmer), Thermogravimetric and differential thermal analyses (NETZSCH STA 409C/CO thermal analyzer), and X-ray diffractometer (Rigaku Miniflex 600).

### Procedure

#### Preparation of complex

The  $[\text{Mn}(\text{bipy})_2][\text{CF}_3\text{SO}_3]_2 \cdot n\text{H}_2\text{O}$  complexes were prepared by the anionic replacement method. A warmed ethanolic solution of *bipy* (0.47 g; 3 mmol, ~4 mL) was added by an aqueous solution of  $\text{Mn}(\text{NO}_3)_2 \cdot 4\text{H}_2\text{O}$  (0.251 g; 1 mmol; ~3 mL). The mixture was filtered, and the aqueous solution of  $\text{KCF}_3\text{SO}_3$  in a slight excess amount (0.75 g; 4 mmol, ~3 mL) was added to the filtrate whereupon the dully greenish precipitate resulted in reducing volume and scratching. The solid was filtered, washed with a minimum of cold water, dried in aeration, and stored in a desiccator.

#### Physical measurements

**Magnetism.** The Magnetic Susceptibility Balance (MSB) of Auto Sherwood Scientific 240V-AC was used to record the magnetic susceptibility in mass ( $\chi_g$ ) of samples. This instrument was calibrated with  $\text{CuSO}_4 \cdot 5\text{H}_2\text{O}$  before running the samples. The powder complex was tightly packed in the Gouy tube till the sign of volume. The difference in mass without and with (electro-)magnet, which reflects the magnetic susceptibility in mass, was then administered. It was converted into molar magnetic susceptibility ( $\chi_M$ ) and then corrected for diamagnetism using Pascal's constant [10-11] to get corrected molar magnetic susceptibility ( $\chi_M'$ ). The effective magnetic moment ( $\mu_{\text{eff}}$ ) was then calculated from the general relationship of the following equation,

$$\mu_{\text{eff}} = 2.828 \sqrt{(\chi_M' \cdot T)} \text{ BM}$$

where T is the temperature of the sample [12-16].

**UV-Vis electronic and infrared spectra.** The spectrophotometer model of Pharmaspec UV 1700 was used to record the UV-Vis electronic spectrum. The sample was spread on a white filter paper closed with a particular thin glass (2 × 2 cm). The fitting was then set in the cell holder, and the spectrum was recorded at 200–1100 nm. An Infrared Spectrophotometer of the FTIR-ABB MB3000 model was used to record the spectrum of the sample. The powdered sample, which was mixed with KBr, was pressed on the cell, and then the spectrum was recorded at 500–4000  $\text{cm}^{-1}$ .

**Metal content and ionic property.** The Atomic Absorption Spectrophotometer of the PinAAcle 900T Perkin Elmer model was used to record the metal content. A conductometer of the Lutron CD-4301 model was used to estimate the conductance property of the complex. It was calibrated with an aqueous solution of 1 M KCl at 25 °C, and several known ionic solutions,  $\text{Ca}(\text{NO}_3)_2$ ,  $\text{Na}_2\text{SO}_4$ ,  $\text{MnSO}_4$ ,  $\text{Mn}(\text{NO}_3)_2$ ,  $\text{FeCl}_3$ , and  $\text{Al}(\text{NO}_3)_3$ , were also recorded for comparison.

**DTG-TGA (Thermogravimetric and differential thermal analyses).** The loss of water molecules and the decomposition of the complex were generated on the Diamond (Perkin Elmer Instruments), and simultaneous DTG-TGA were recorded by a NETZSCH STA 409C/CO thermal analyzer model with the rate of 10 °C/min.

**Powder diffraction.** The Rigaku Miniflex 600 40 kW 15 mA Benchtop Diffractometer with  $\text{CuK}\alpha$ ,  $\lambda = 1.5406 \text{ \AA}$  was used to record the diffractogram of the complex. The sample was spread on a special glass plate and set on the cell holder. The diffractogram was then recorded in a scan mode at 2–90° of  $2\theta$  within the interval of 0.04 steps per 4 sec for 2 h. The recorded diffractogram was then refined following the Le Bail method within 10–50° of  $2\theta$ , which was run within 50 cycles.

#### Determination of antibacterial activity

Antibacterial activity of the complex was tested against *S. aureus* (ATCC 25924) and *E. coli* (ATCC 35218) according to the agar disk-dilution method in Nutrient Agar (NA) and Nutrient Broth (NB) as media and chloramphenicol as a standard antibacterial agent

(positive control). It was performed at various concentrations of the complex, 125, 250, 500, and 1000 µg/mL. The observation of the inhibition zone (in mm) was done every 3 h during 24 h of incubation. The diameter of the inhibition zone was measured by measuring the distance from the edge of the test sample to the circular boundary of the inhibition zone using a caliper (accuracy 0.02 mm) on 3 sides of the sample [17-18].

## ■ RESULTS AND DISCUSSION

### Conductance, AAS, DTG-TGA and Chemical Formula

The interactions of the clear solutions of *bipy* and manganese(II) produced a dully-greenish solution of the corresponding new compound, which is precipitated by the addition of the saturated excessive triflate solution. The equivalent electrical conductance of this compound was measured together with some other known simple salts, and the results are collected in Table 1.

It is observed that the complex might be classified in the range of the three ions per molecule, and therefore the stoichiometric empirical formula of  $[\text{Mn}(\text{bipy})_n](\text{CF}_3\text{SO}_3)_2 \cdot x\text{H}_2\text{O}$  (where  $n = 3$ ) is then worth proposed, reflecting the uncoordinated anionic triflate.

As shown in Fig. 1 and Table 2, the loss of mass of about 10.59% in the first stage at 100–160 °C is believed to be due to the loss of water lattice [19], being 5.5 H<sub>2</sub>O (ca. 10.75%). While the remaining stages are not particularly analyzed, the DTG curve suggests that 3-*bipy* is lost in three stages, and the residue at above 540 °C is believed to be manganese oxides as the slow conversion Mn<sub>2</sub>O<sub>3</sub> to Mn<sub>3</sub>O<sub>4</sub> [20]. Together with the metal content, Mn, obtained from atomic absorption spectral data, 0.05976% (ca. 0.05967%), this suggests confirming the proposed formula of  $[\text{Mn}(\text{bipy})_3](\text{CF}_3\text{SO}_3)_2 \cdot 5.5\text{H}_2\text{O}$ .

### Magnetism

The magnetic moment of the complex is calculated from the molar magnetic susceptibility data which were collected by the measurement for the two separated preparation (Sample 1 and 2) was found to be 6.17 and 5.87 BM at 298 K, respectively (Table 3), being normal paramagnetic nature. This reflects the spin-only value ( $\mu_s$ ), corresponding to five unpaired electrons in the metal ion, and it is the normal value in an octahedral geometry, as observed in some literature to be 5.89–6.16 BM for various compounds [1,9,21-23].

**Table 1.** Equivalent electric conductance of the aqueous solutions of  $[\text{Mn}(\text{bipy})_n](\text{CF}_3\text{SO}_3)_2 \cdot x\text{H}_2\text{O}$  and some known salts (some data, NH<sub>4</sub><sup>+</sup>, Ca<sup>2+</sup>, Al<sup>3+</sup>, and Fe<sup>3+</sup>, are confirmed to references)

Compounds	Equivalent conductance (Λc) Ω <sup>-1</sup> cm <sup>2</sup> mol <sup>-1</sup>	Ratio of cation/anion	Number of ions per molecule	Reference
NH <sub>4</sub> Cl	70–78	1:1	2	[4]
MnSO <sub>4</sub>	112.366	1:1	2	
Ca(NO <sub>3</sub> ) <sub>2</sub>	379.355	1:2	3	[5]
Mn(NO <sub>3</sub> ) <sub>2</sub>	207.777	1:2	3	
Na <sub>2</sub> SO <sub>4</sub>	214.39	2:1	3	
Al(NO <sub>3</sub> ) <sub>3</sub>	510–519	1:3	4	[5-7]
FeCl <sub>3</sub>	477–573	1:3	4	[5-7]
$[\text{Mn}(\text{bipy})_n](\text{CF}_3\text{SO}_3)_2 \cdot x\text{H}_2\text{O}$	261.202	1:2	3	

**Table 2.** The detailed formula of the complex following the metal TGA content

Proposed complex	H <sub>2</sub> O content		AAS-Mn content (mg/g)	
	Calculated	TGA (%)	Calculated	Found
$[\text{Mn}(\text{bipy})_3](\text{CF}_3\text{SO}_3)_2 \cdot 5\text{H}_2\text{O}$	9.87		60.26	
$[\text{Mn}(\text{bipy})_3](\text{CF}_3\text{SO}_3)_2 \cdot 5.5\text{H}_2\text{O}$	10.75	10.59	59.67	59.76
$[\text{Mn}(\text{bipy})_3](\text{CF}_3\text{SO}_3)_2 \cdot 6\text{H}_2\text{O}$	11.61		59.09	

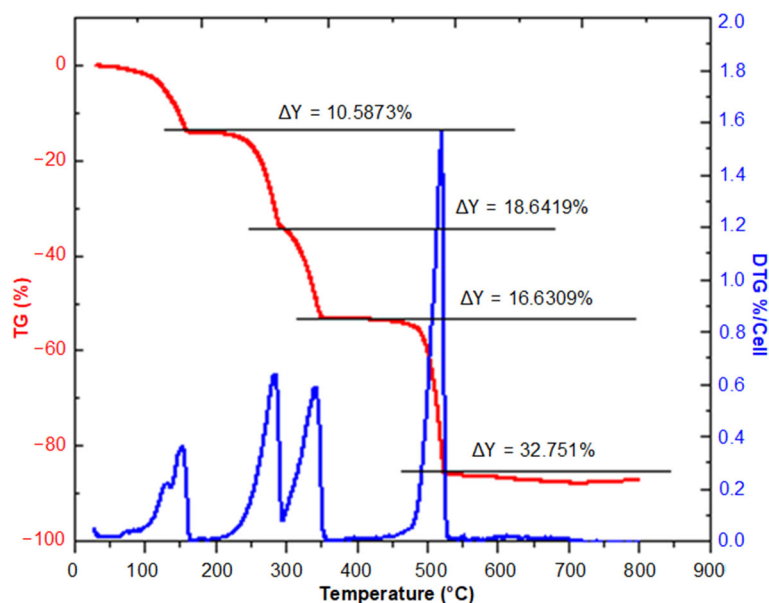


Fig 1. The DTG-TGA of  $[\text{Mn}(\text{bipy})_3](\text{CF}_3\text{SO}_3)_2 \cdot x\text{H}_2\text{O}$  at 30–900 °C

Much lower values of several Mn(II) complexes, however, have been reported to be only 4.24 to 4.34 BM at 77–303 K [24], 4.65 BM [25], and 5.12 BM [26].

### Electronic Spectrum

The normal high-spin nature, as confirmed by the magnetic data, suggests to the ground state of the sextet,  ${}^6A_{1g}$ , and as no other sextet excited state is possible, there are no spin-allowed transitions, but the spin-forbidden transitions to quartet states perform the absorption bands and consequently giving rise to very low intensities. The UV-Vis spectra of the powder complex and its solution (inset), as depicted in Fig. 2, exhibit strong ligand absorptions of the  $\pi \rightarrow \pi^*$  and  $n \rightarrow \pi^*$  at  $\sim 250$  nm ( $40000 \text{ cm}^{-1}$ ) and 290 nm ( $34500 \text{ cm}^{-1}$ ), respectively, being comparable to the 1,10-phenanthroline ligand [26]. This strong ligand absorption is down to the visible area, and as a result, the  $d-d$  spin-forbidden ligand field transitions, which are very low intensities, are not well resolved due to the mask of the tail absorption band as reported by Hariyanto et al. [27].

Following the Tanabe-Sugano diagram for  $\text{MnF}_2$  and comparably observed for other literature at the range  $19500\text{--}42000 \text{ cm}^{-1}$  [28–29], those two strong ligand bands should mask all possible  $d-d$  spin-forbidden transitions [ $\nu_1\text{--}\nu_6$ :  ${}^6A_{1g} \rightarrow {}^4T_{1g}({}^4G)$ ;  ${}^6A_{1g} \rightarrow {}^4T_{2g}({}^4G)$ ;  ${}^6A_{1g} \rightarrow {}^4E_g({}^4G)$ ,  ${}^4A_{1g}({}^4G)$ ;  ${}^6A_{1g} \rightarrow {}^4T_{2g}({}^4D)$ ; and  ${}^6A_{1g} \rightarrow {}^4E_g({}^4D)$ ,  ${}^4T_{1g}({}^4P)$ ; and

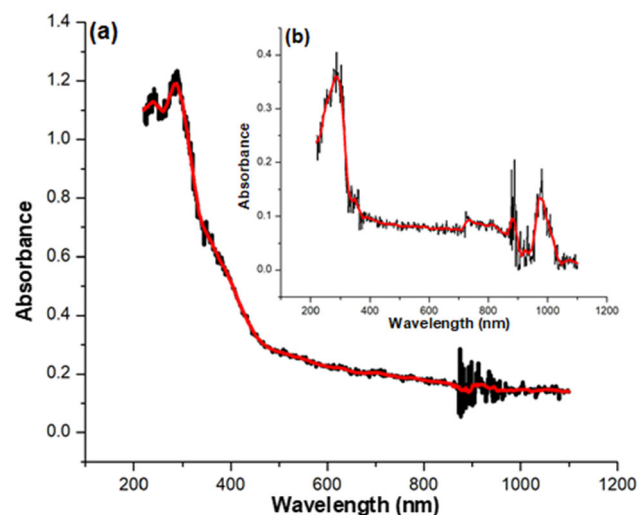


Fig 2. Electronic spectra of  $[\text{Mn}(\text{bipy})_3](\text{CF}_3\text{SO}_3)_2 \cdot 5.5\text{H}_2\text{O}$ : (a) powder; (b) in solution (inset)

${}^6A_{1g} \rightarrow {}^4T_{1g}({}^4F)$ , respectively] which are presumably in the range  $19000\text{--}21000 \text{ cm}^{-1}$  ( $\nu_1$ ),  $24000\text{--}25000 \text{ cm}^{-1}$  ( $\nu_2$ ),  $26000\text{--}28000 \text{ cm}^{-1}$  ( $\nu_3$ ),  $\sim 30000$ ,  $\sim 33500 \text{ cm}^{-1}$  ( $\nu_4$ ),  $\sim 36500 \text{ cm}^{-1}$  ( $\nu_5$ ), and  $39000\text{--}41000 \text{ cm}^{-1}$  ( $\nu_6$ ), respectively. However, the strong-broad shoulder centered at about 355 nm ( $28160 \text{ cm}^{-1}$ ) for the solid spectrum, which might be split into two at 355 nm ( $28160 \text{ cm}^{-1}$ ) and 385 nm ( $25970 \text{ cm}^{-1}$ ) in the solution spectrum (Fig. 2b), strongly suggest to be  $\nu_3$  and  $\nu_2$ , respectively [30]. The similarity of the spectral pattern of

the powder and that in solution reflects the stability of this complex.

### Infrared Spectra

The IR spectral profile of the complex and the anionic triflate ( $\text{CF}_3\text{SO}_3$ ) are shown in Fig. 3. Direct comparison of the two might be made, and thus, the main modes of triflate should be readily assigned in the range of about  $1200\text{--}500\text{ cm}^{-1}$ , in which the detailed modes of vibrations, symmetric-/asymmetric-stretching modes of  $\text{SO}_3$  ( $\sim 1250\text{ cm}^{-1}$ ) and  $\text{CF}_3$  ( $1000\text{ cm}^{-1}$ ), symmetry deformations of  $\text{C-F}_3$  ( $\sim 750\text{ cm}^{-1}$ ) and  $\text{SO}_3$  ( $\sim 625\text{ cm}^{-1}$ ) have been reported in the previous references [2,4-5,27,31-32]. No indicative coordination with the metal is suggested for this anion, consistent with the formula proposed.

In the case of *bipy*-chelation, the typical ring modes ( $\nu_{\text{C-C}}$ ;  $\nu_{\text{C-N}}$ ;  $\text{C-H}$ ; *bipy* 'breathing') are to be in the range of  $1625\text{--}800\text{ cm}^{-1}$ . The broad stretching mode at  $3500\text{--}3600\text{ cm}^{-1}$  is due to the symmetric-/anti symmetric-stretching modes of  $\text{-OH}$  of the  $\text{H}_2\text{O}$  lattice as indicated in the TG-DTA data. Another band at  $3000\text{ cm}^{-1}$  is due to the stretching vibration of  $\text{C-H}$  bonds of pyridine rings [20,33].

### SEM, EDX, and Powder XRD

As shown in Fig. 4, the complex indicates more or less the bulky poly-crystalline rather than amorphous type (SEM, (a)), with all main elemental content (C, N, O, F, S, and Mn) except for hydrogen (EDX, (b)). It is confirmed by the corresponding diffractogram profile (Fig. 5), showing no broad but sharp peaks.

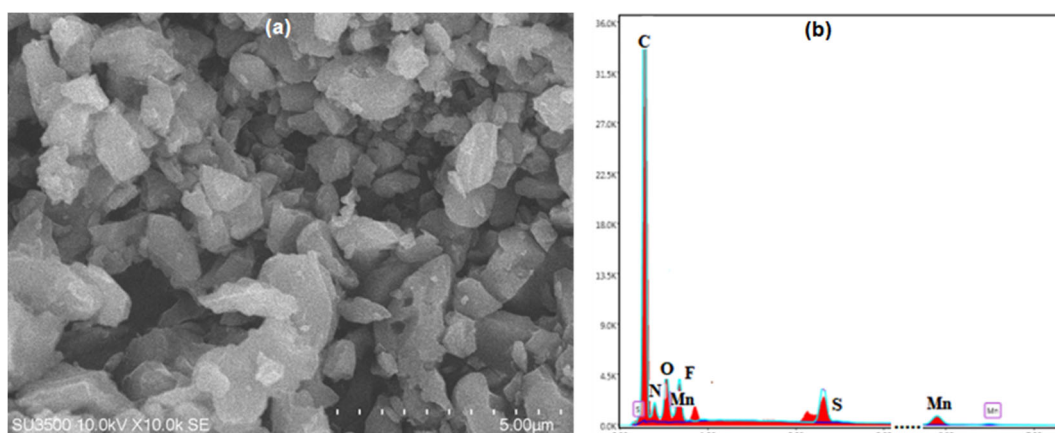


**Fig 4.** SEM photograph of  $[\text{Mn}(\text{bipy})_3](\text{CF}_3\text{SO}_3)_2 \cdot 5.5\text{H}_2\text{O}$  at a magnification of  $50.000\times$  (a) showing the crystalline type and EDX (b) showing elemental content

### X-Ray Powder Diffraction and Structural Refinement

The crystal structure of  $[\text{Mn}(\text{bipy})_3](\text{ClO}_4)_2$  has been established through different preparation of single crystal to signify the coordination of  $\text{Mn-N}(\text{bipy})$ . Surprisingly, two types of symmetry and space groups are observed [17,34-35]. For this reason, those data might be employed as references to refine the P-XRD of  $[\text{Mn}(\text{bipy})_3](\text{CF}_3\text{SO}_3)_2 \cdot 5.5\text{H}_2\text{O}$ , as recorded in Fig. 5.

The corresponding diffractogram is shown in Fig. 5. It can be seen that the red-full line of the Le Bail refinement program does touch almost all black points (+)

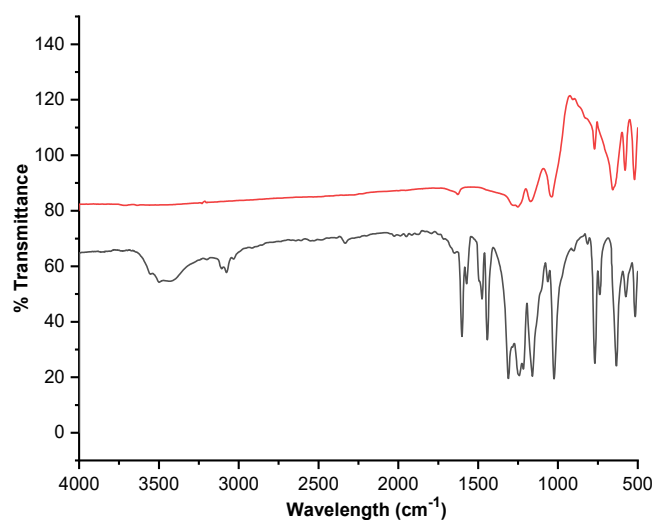


**Fig 3.** IR Spectra of  $[\text{Mn}(\text{bipy})_3](\text{CF}_3\text{SO}_3)_2 \cdot 5.5\text{H}_2\text{O}$  (black) and  $\text{KCF}_3\text{SO}_3$  (red). Note: Relative transmittance (in %) only significant for each spectrum

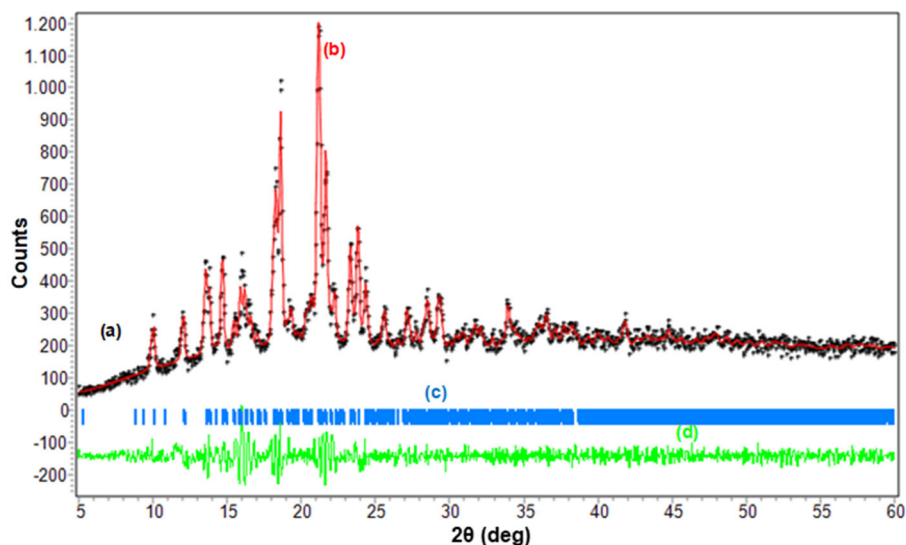


**Fig 5.** P-XRD profile of  $[\text{Mn}(\text{bipy})_3](\text{CF}_3\text{SO}_3)_2 \cdot 5.5\text{H}_2\text{O}$  (a-black), the refinement on monoclinic symmetry of  $P_{21}/c$  (b-red) with its position of  $2\theta$  (c-blue), and the intensity difference between the black and the red lines (d-green)

**Table 4.** Crystallography data of  $[\text{Mn}(\text{bipy})_3]\text{X}_2^{\text{a}}$  and  $[\text{Mn}(\text{bipy})_2\text{X}_2]^{\text{b}}$ ; ( $\text{X} = \text{CF}_3\text{SO}_3$ ;  $\text{ClO}_4$ )

Complex	$\text{X} = \text{CF}_3\text{SO}_3^{\text{a}}$	$\text{X} = \text{ClO}_4^{\text{a}}$ [17]	$\text{X} = \text{ClO}_4^{\text{b}}$ [17]	$\text{X} = \text{ClO}_4^{\text{a}}$ [34]	$\text{X} = \text{ClO}_4^{\text{a}}$ [35]
Color	Greenish-yellowish	Yellow	Green	Golden yellow	Pale yellow
Symmetry	Monoclinic	Monoclinic	Monoclinic	Triclinic	Triclinic
Space Group	$P_{21}/c$	$P_{21}/c$	$P_{21}/n$	$P\bar{1}$	$P\bar{1}$
a (Å)	18.63498	18.6642	8.2272	8.133 (2)	9.535(2)
b (Å)	7.10764	7.932	13.3691(9)	11.056(2)	13.194(3)
c (Å)	21.4993	21.4812	21.0132(14)	18.658(5)	14.854(3)
a (°)	90.0	90.0	90.0	91.02(2)	107.26(3)
$\beta$ (°)	99.6889	102.9	100.1(3)	91.02(2)	107.26(3)
$\gamma$ (°)	90.0	90.0	90.0	99.77(2)	91.19(3)
V (Å <sup>3</sup> )	2806.9936	3099.3	2275.8(3)	1613.1(7)	1770.2(7)
Z	4			2	2
The figure of Merit:					
$R_p$	6.07	-			
$R_{wp}$	9.25	-			
$R_{exp}$	8.47	-			
GOF	1.192	1.025	1.062	-	1.020
Bragg R-Factor	0.03	-		-	

of experimental data within the expected symmetry and space group model (blue-bar lines). The different intensity between the two experimental points and the refinement line is almost flat green-line, and this demonstrates an acceptable fitting model. The detailed lattice parameters of the structure due to the fitting are then collected in Table 4, together with the relevant data for some known single crystals of the same cations [17,34-

35]. The low figures of merit strongly suggest acceptable refinement, and thus, this complex prepared in this work might be classified as monoclinic symmetry of  $P_{21}/c$ .

#### Antibacterial Activity Test

Antibacterial activities of the complex were tested against *S. aureus* and *E. coli* bacteria with chloramphenicol as a positive control according to the

agar disc-dilution method in Nutrient Agar (NA) and Nutrient Broth (NB) [18]. A total number of 53 bacterial incubations in Petri dishes were prepared, and the two selected inhibition zone sizes of images of them for *S. aureus* at 250 µg/mL are shown in Fig. 6.

All numeric data of the concentration of the complex, and the diameter of the inhibition zone (in mm) with time (in h) are summarized and described graphically in Fig. 7 and Fig. 8.

It was found that the complex exhibits inhibition of the growth activity for both bacteria, *S. aureus* and *E. coli*. After the *two-way* ANOVA followed by Duncan (multiple distances) test, it can be concluded that the concentration of complex as a bacterial inhibitor, and incubation time, both affect the activity of the two bacteria simultaneously. Following the Duncan (multiple distances) test, it was found that the most effective in inhibiting bacterial growth is at 1000 µg/mL as the minimum inhibition

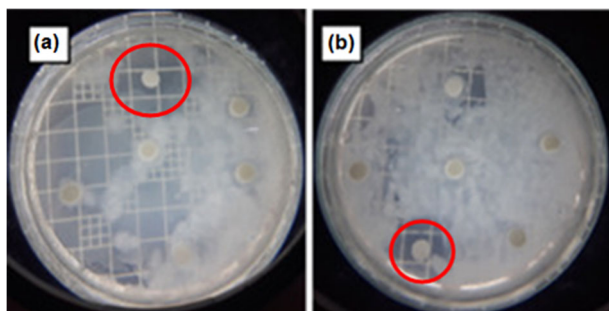


**Fig 6.** Selected images of bacterial incubation in petri dishes with a clear inhibition zone (red circle) for *S. aureus* at 250 µg/mL

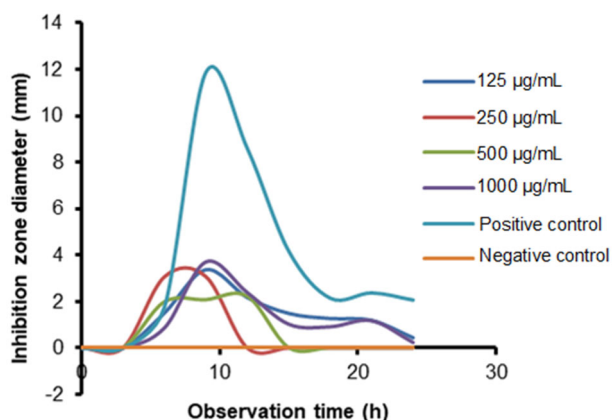


**Fig 7.** Graph of a diameter of the inhibition zone (in mm) at various concentrations of the complex against the time of *S. aureus* activity (in h)

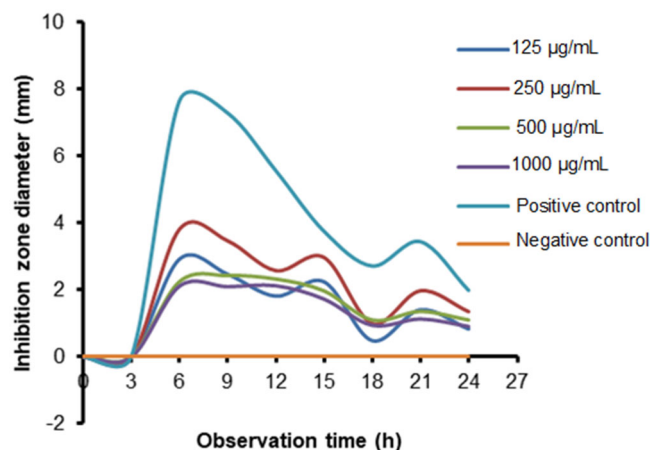


**Fig 8.** Graph of the diameter of the inhibition zone (in mm) at various concentrations of the complex against the time of *E. coli* activity (in h)

concentration (MIC) with the death phase within 9 h against the *S. aureus*, and at 250 µg/mL (MIC) with the death phase within 6–15 h against the *E. coli*.

In comparison to the simple compound,  $\text{MnCO}_3$  [8] and  $\text{Mn}(\text{ClO}_4)_2$  [17], for example, there is no antibacterial activity. Thus, in the light of chelation theory, it has been proposed that chelation of *bipy* might considerably reduce the charge of the metal ion, while the formation of a hydrogen bond through the anionic triflate might result in interference with the normal cell process [8-9].

## CONCLUSION

In this work, the powdered complex of  $[\text{Mn}(\text{bipy})_3](\text{CF}_3\text{SO}_3)_2 \cdot 5.5\text{H}_2\text{O}$ , has been isolated as strongly confirmed by AAS, DTG-TGA, conductance, magnetism, UV-Vis and IR spectral properties. The corresponding cell parameters have been reviewed by Le-Bail refinement to the P-XRD diffractogram, which is found to fit the monoclinic symmetry of the  $P_{21/c}$  space group. Its antibacterial activity against *S. aureus* and *E. coli* bacteria is found to show inhibition of bacterial growth.

## ACKNOWLEDGMENTS

Authors greatly acknowledge the Faculty of Mathematics and Science, Yogyakarta State of University, due to the financial support (Contract Number: B/186/UN34.13/PM.01.01/2020).

## ■ REFERENCES

- [1] Sugiyarto, K.H., Saputra, H.W., Permanasari, L., and Kusumawardani, C., 2017, Structural analysis of powder complex of  $[\text{Mn}(\text{phen})_3](\text{CF}_3\text{SO}_3)_2 \cdot 6.5\text{H}_2\text{O}$ , *AIP Conf. Proc.*, 1847, 040006.
- [2] Sugiyarto, K.H., Kusumawardani, C., Sutrisno, H., and Wibowo, M.W.A., 2018, Structural analysis of powdered manganese(II) of 1,10-phenanthroline (phen) as ligand and trifluoroacetate (TFA) as counter anion, *Orient. J. Chem.*, 34 (2), 735–742.
- [3] Kusumawardani, C., Kainastiti, F., and Sugiyarto, K.H., 2018, Structural analysis of powder complex of  $\text{Cu}(\text{bipy})_3(\text{CF}_3\text{SO}_3)_2(\text{H}_2\text{O})_x$  ( $x = 0.5, 1$ ), *Chiang Mai J. Sci.*, 45 (4), 1944–1952.
- [4] Sugiyarto, K.H., Kusumawardani, C., and Wulandari, K.E., 2018, Synthesis and structural analysis of powder complex of tris(bipyridine)cobalt(II) trifluoromethanesulfonate octahydrate, *Indones. J. Chem.*, 18 (4), 696–701.
- [5] Sutrisno, H., Kusumawardani, C., Rananggana, R.Y., and Sugiyarto, K.H., 2018, Structural analysis of powder tris(phenanthroline)nickel(II) trifluoroacetate, *Chiang Mai J. Sci.*, 45 (7), 2768–2778.
- [6] Sugiyarto, K.H., Kusumawardani, C., Wigati, H., and Sutrisno, H., 2019, Structural study of the powder complex of  $\text{Cu}(\text{II})$ -1,10-phenanthroline-trifluoroacetate, *Orient. J. Chem.*, 35 (1), 325–331.
- [7] Sugiyarto, K.H., Louise, I.S.Y., and Wilujeng, S.S., 2020, Preparation and powder XRD analysis of tris(2,2'-bipyridine)nickel(II) trifluoroacetate, *Indones. J. Chem.*, 20 (4), 833–841.
- [8] Uddin, S., Saddam Hossain, M., Abdul Latif, M., Rabiul karim, M., Mohapatra, R.K., and Kudrat-E-Zahan, 2019, Antimicrobial activity of Mn complexes incorporating Schiff bases: A short review, *Am. J. Heterocycl. Chem.*, 5 (2), 27–36.
- [9] Singh, B.K., Mishra, P., Prakash, A., and Bhojak, N., 2017, Spectroscopic, electrochemical and biological studies of the metal complexes of the Schiff base derived from pyrrole-2-carbaldehyde and ethylenediamine, *Arabian J. Chem.*, 10, S472–S483.
- [10] Bain, G.A., and Berry, J.F., 2008, Diamagnetic corrections and Pascal's constants, *J. Chem. Educ.*, 85 (4), 532–536.
- [11] Dalal, M.A., 2017, "Magnetic Properties of Transition Metal Complexes" in *Textbook of Inorganic Chemistry*, Volume 1, Dalal Institute, India, 342–386.
- [12] e-PG Pathshala, 2021, *Inorganic Chemistry-II: Metal-Ligand Bonding, Electronic Spectra and Magnetic Properties of Transition Metal Complexes*, [http://epgp.inflibnet.ac.in/epgpdata/uploads/epgp\\_content/chemistry/07.inorganic\\_chemistry-ii/33\\_anomalous\\_magnetic\\_moment/et/8821\\_et\\_et.pdf](http://epgp.inflibnet.ac.in/epgpdata/uploads/epgp_content/chemistry/07.inorganic_chemistry-ii/33_anomalous_magnetic_moment/et/8821_et_et.pdf), accessed 15 December 2021.
- [13] Chemistry LibreTexts, 2020, *Magnetism*. [https://chem.libretexts.org/Bookshelves/Inorganic\\_Chemistry/Supplemental\\_Modules\\_and\\_Websites\\_\(Inorganic\\_Chemistry\)/Crystal\\_Field\\_Theory/Magnetism](https://chem.libretexts.org/Bookshelves/Inorganic_Chemistry/Supplemental_Modules_and_Websites_(Inorganic_Chemistry)/Crystal_Field_Theory/Magnetism), accessed 15 December 2021.
- [14] Chemistry LibreTexts, 2021, *Magnetic Susceptibility and the Spin-only Formula*, [https://chem.libretexts.org/Bookshelves/Inorganic\\_Chemistry/Map%3A\\_Inorganic\\_Chemistry\\_\(Houusecroft\)/20%3A\\_d-Block\\_Metal\\_Chemistry\\_-\\_Coordination\\_Complexes/20.10%3A\\_Magnetic\\_Properties/20.10A%3A\\_Magnetic\\_Susceptibility\\_and\\_the\\_Spin-only\\_Formula](https://chem.libretexts.org/Bookshelves/Inorganic_Chemistry/Map%3A_Inorganic_Chemistry_(Houusecroft)/20%3A_d-Block_Metal_Chemistry_-_Coordination_Complexes/20.10%3A_Magnetic_Properties/20.10A%3A_Magnetic_Susceptibility_and_the_Spin-only_Formula), accessed 15 December 2021.
- [15] Chemistry LibreTexts, 2020, *Magnetic Moments of Transition Metals*, [https://chem.libretexts.org/Bookshelves/Inorganic\\_Chemistry/Supplemental\\_Modules\\_and\\_Websites\\_\(Inorganic\\_Chemistry\)/Crystal\\_Field\\_Theory/Magnetic\\_Moments\\_of\\_Transition\\_Metals](https://chem.libretexts.org/Bookshelves/Inorganic_Chemistry/Supplemental_Modules_and_Websites_(Inorganic_Chemistry)/Crystal_Field_Theory/Magnetic_Moments_of_Transition_Metals), accessed 15 December 2021.
- [16] LibreTexts™, 2021, *Jahn-Teller Effect*, [https://chem.libretexts.org/Bookshelves/Inorganic\\_Chemistry/Book%3A\\_Introduction\\_to\\_Inorganic\\_Chemistry\\_\(Wikibook\)/05%3A\\_Coordination\\_Chemistry\\_and\\_Crystal\\_Field\\_Theory/5.08%3A\\_Jahn-Teller\\_Effect](https://chem.libretexts.org/Bookshelves/Inorganic_Chemistry/Book%3A_Introduction_to_Inorganic_Chemistry_(Wikibook)/05%3A_Coordination_Chemistry_and_Crystal_Field_Theory/5.08%3A_Jahn-Teller_Effect), accessed 27 January 2022.
- [17] Kani, I., Atlier, O., and Güven, K., 2016, Mn(II) complexes with bipyridine, phenanthroline and benzoic acid: Biological and catalase-like activity, *J. Chem. Sci.*, 128 (4), 523–536.

- [18] Balouiri, M., Sadiki, M., and Ibsouda, S.K., 2016, Methods for *in vitro* evaluating antimicrobial activity: A review, *J. Pharm. Anal.*, 6 (2), 71–79.
- [19] Dubey, R.K., Paswan, S., Anjum, A., and Singh, A.P., 2019, Synthesis and spectroscopic characterization of lanthanide complexes derived from 9,10-phenanthrenequinone and Schiff base ligands containing N, O donor atoms, *Indian J. Chem., Sect. A*, 58 (4), 446–453.
- [20] Czakis-Sulikowska, D., and Czyłkowska, A., 2003, Thermal and other properties of complexes of Mn(II), Co(II) and Ni(II) with 2,2'-bipyridine and trichloroacetates, *J. Therm. Anal. Calorim.*, 74 (1), 349–360.
- [21] Verma, R., 2017, Synthesis and characterisation of manganese(II) complexes with semicarbazide and thiosemicarbazide based ligands, *Int. J. Pharm. Sci. Res.*, 8 (3), 1504–1513.
- [22] Waheed, E.J., Farhan, M.A., and Hameed, G.F., 2019, Synthesis and characterization of new manganese(II), cobalt(II), cadmium(II) and mercury(II) complexes with ligand [N-(3-acetylphenylcarbamoithiyl)-2-chloroacetamide] and their antibacterial studies, *J. Phys.: Conf. Ser.*, 1234, 012096.
- [23] Fayyadh, B.M., Basim Abd, N.A., and Sarhan, B.M., 2022, Synthesis and characterization of new Mn(II), Co(II), Cd(II) and Hg(II) complexes with ligand [N-(pyrimidin-2-ylcarbamoithiyl)benzamide] and their anti-bacterial study, *IOP Conf. Ser.: Earth Environ. Sci.*, 1029, 012030.
- [24] Ferenc, W., Dariusz, O., Sarzyński, J., and Gluchowska, H., 2020, Complexes of Mn(II), Co(II), Ni(II), Cu(II) and Zn(II) with ligand formed by condensation reaction of isatin with glutamic acid, *Eletica Quim.*, 45 (3), 12–27.
- [25] Shaker, S.A., Khaledi, H., Cheah, S.C., and Mohd Ali, H., 2016, New Mn(II), Ni(II), Cd(II), Pb(II) complexes with 2-methylbenzimidazole and other ligands. Synthesis, spectroscopic characterization, crystal structure, magnetic susceptibility and biological activity studies, *Arabian J. Chem.*, 9, S1943–S1950.
- [26] Fayad, N.K., Al-Noor, T.H., Mahmood, A.A., and Malih, I.K., 2013, Synthesis, characterization, and antibacterial studies of Mn(II), Fe(II), Co(II), Ni(II), Cu(II) and Cd(II) mixed- ligand complexes containing amino acid (L-Valine) and (1,10-phenanthroline), *Chem. Mater. Res.*, 3 (5), 66–73.
- [27] Hariyanto, N.A., Hanapi, A., Ningsih, R., and Solawati, W., 2021, Synthesis and Characterization of Mn(II) Complex Compounds with Ligand Schiff Base 2-methoxy-6((4-methoxyphenylimino)methyl) phenol, *The 11<sup>th</sup> International Conference on Green Technology*, Universitas Islam Negeri Maulana Malik Ibrahim Malang, 26 October 2021, 29–32.
- [28] Lever, A.B.P., 1968, “Crystal Field Spectra” in *Inorganic Electronic Spectroscopy*, 1<sup>st</sup> Ed., Elsevier Science Publisher, Amsterdam, 249–360.
- [29] Dalal, M.A., 2017, “Electronic Spectra of Transition Metal Complexes” in *Textbook of Inorganic Chemistry*, Volume 1, Dalal Institute, India, 214–341.
- [30] Chandra, S., and Pipil, P., 2013, Spectral studies of transition metal complexes with 25,26-dioxo-1,6,12,17,23,24-hexaazacyclohexacosane-1,5,12,16-tetraene macrocyclic ligand (L), *Open J. Inorg. Chem.*, 3 (4), 38775.
- [31] Ignat'ev, N.V., Barthen, P., Kucheryna, A., Willner, H., and Sartori, P., 2012, A convenient synthesis of triflate anion ionic liquids and their properties, *Molecules*, 17 (5), 5319–5338.
- [32] Kusumawardani, C., Permanasari, L., Fatonah, S.D., and Sugiyarto, K.H., 2017, Structural analysis of powder complex of tris(1,10-phenanthroline)copper(II) trifluoromethane sulfonate dihydrate, *Orient. J. Chem.*, 33 (6), 2841–2847.
- [33] Czakis-Sulikowska, D., and Czyłkowska, A., 2005, New 2,2'-bipyridine-chloroacetato complexes of transition metals(II), *J. Therm. Anal. Calorim.*, 82 (1), 69–75.
- [34] Chen, X.M., Wang, R.Q., and Xu, Z.T., 1995, Tris(2,2'-bipyridine)manganese(II) perchlorate hemihydrate, *Acta Crystallogr., Sect. C: Struct. Chem.*, 51 (5), 820–822.
- [35] Yu, X.L., Tong, Y.X., Chen, X.M., and Mak, T.C.W., 1997, Crystal structure of [Mn(bpy)<sub>3</sub>](ClO<sub>4</sub>)<sub>2</sub>·0.5(bpy) (bpy=2,2'-bipyridine), *J. Chem. Crystallogr.*, 27 (7), 441–444.